ingegneria sismica
International Journal of Earthquake Engineering
Anno XXXV – Num. 3

NUMERICAL STUDY OF CFT COLUMNS UNDER AXIAL, ECCENTRIC AND LATERAL CYCLIC LOADING

Ebrahim Farajpourbonab[1]

[1]Department of Civil Engineering, University of Pune, Pune, (M.S.), India

SUMMARY: *This paper presents a numerical study of the various steel tube sections of Concrete Filled steel Tube (CFT) columns under axial, eccentric and lateral cyclic loading based on the Ansys standard solver. The feasibility and accuracy of the numerical method was verified by comparing the numerical results with the experimental observations. Because of inconvenient performance of traditional CFT columns, new steel wall sections proposed in the current study to improve the strength and hysteresis behavior of these columns. For this purpose, eight CFT samples, including two polygons soffit sections, two polygons extrados sections, square section, circular section, circular section with reinforced bars, and octagon section with stiffeners proposed for the analyses. The results of analyses indicate the increase in strength and ductility of the suggested sections in comparison with traditional ones and they can be used in the seismic region and practical engineering applications.*

KEYWORDS: *CFT column, compressive strength, Octagon and Polygons steel sections, FE analysis, hysteretic behavior*

1 Introduction

Composite and hybrid structures offer many advantages for seismic design. They significantly increase the strength and stiffness of the building at little increase in cost. [Mete et al., 2016] mentioned that this important feature made Concrete Filled steel Tube (CFT) columns more appropriate for high-rise constructions in the high seismic areas and therefore the filled tubular columns require more attention. [Rides et al., 1996] by designing an archetype of 20-story building using two difference options represented the superiority of CFT column system construction. They found that because of reduction of steel weight, total cost of CFT column will be reduced. [Morino et al., 2001] studied the cost performance of Concrete Filled steel Tube (CFT) column system by theme structures design with un-braced building frames (10, 24 and 40-story) made of steel or CFT systems. They found that the cost of the CFT major frames is 5 to 7% less than that of the steel frames; the cost total building for the CFT system is 1% less than that of the steel system and if the cost of major structural frame is supposed to occupy 15% of the cost of total building; with the increase of the number of stories, the cost excellence of the CFT system becomes greater. [Hamidian et al., 2016] mentioned that the inherent advantages of CFT columns were proven in Hansin-Awaji Japan's earthquake. In this earthquake, most of the steel structures and reinforced concrete were heavily damaged due to the local buckling and shear failures of columns while, CFT structures avoided collapse and the main reason was the composite action between steel tube and concrete core of CFT columns. The concrete in this type of composite column can be plain (CFT) or reinforced with steel bar (RCFT). Current studies such as [Xiamuxi and Hasegawa, 2011-2012, Endo et al., 2014, and Hua et al., 2005] show that RCFT (Reinforced Concrete Filled Tube) columns have better performance regarding moderate and severe earthquake excitations, higher toughness, and ductility in comparison with CFT columns.

Corresponding author: Ebrahim Farajpourbonab, Department of Civil Engineering, University of Pune, India.
Email:farajpourbonab@gmail.com

[Uenaka, 2014] showed that the axial load capacity of elliptical CFT columns could be estimated by the equation including confinement effect of smaller diameter direction. [Schneider, 1998] have presented experimental and analytical studies on the behavior of short concrete in-filled steel tubular columns under concentric loads. Experimental results suggested that the circular tubes offer substantial post-yield strength and stiffness. [Qin and Xiao, 2013, Schnabl et al., 2015, and Chitawadagi et al., 2010] found that the ratio of diameter to thickness and the material properties strongly affect the seismic behavior of CFT columns. Better performance can be observed for CFT columns with smaller tube diameter to thickness ratio and higher material strengths.

A long column is sensitive to eccentric loading effects and initial out-of-straightness. [Gardner et al., 1992, Rangan and Joyce, 1992, Gopal and Manoharan, 2006, Galano and Vignoli, 2008, Chithira and Baskar, 2012] mentioned that the failure mechanism of long columns due to eccentric loading will be similar to the concentric case, except that failure will occur at a smaller load and the failure load will decrease with an increase in eccentricity. However, the axial load and bending capacities of CFST could be improved by providing sufficient internal stiffening method as discussed in details by [Clotilda et al., 2010-2011]. Clotilda et al., 2016 have conducted an experimental investigation into the structural behavior of eccentrically loaded concrete filled, thin walled, steel tubular slender column with tab stiffeners (CFST). It was observed that all specimens failed mainly by overall buckling and, the compressive strength and bending strength of the specimens decreases as the applied load eccentricity increases.

[Dario *et al., 2017]* have investigated the Assessment of the efficiency of seismic design for structural robustness of rc structures. The aim of this work is to assess the efficiency of the seismic detailing to ensure robustness of structures not directly designed against progressive and disproportionate collapse. The assessment is based on the comparison of two distinct design of the same structure: in the first case the seismic action is considered, while in the second one the seismic action is neglected. Both the structures are subjected to a column removal and their response after this exceptional event is evaluated. Three different configurations are tested removing respectively an internal, an edge and a corner column placed at the ground floor level. The obtained results show the improvement achievable, in terms of structural robustness, adopting seismic detailing, highlighting the importance of a seismic-oriented design also in the prevention of collapse due to accidental actions. [Montuori and Piluso, 2015] have developed a fibre model to predict the ultimate behavior of Concrete Filled Tubular (CFT) members subjected to non-uniform bending. The presented fibre model accounts for all the effects influencing the ultimate behavior of composite members, such as local buckling, confining effects on concrete, bi-axial stress state of the steel plate elements constituting the hollow profile and hardening of its corners due to cold forming process. The results have confirmed the high attitude of such structural members for their application in seismic resistant structures, being both strength and ductility highly suitable and satisfactory for the role of dissipative zones. [Cavaleri et al., 2017] have proposed a selected review of some of the most important NSC (Normal Strength Concrete) and HSC (High Strength Concrete) confinement models, presenting the analytical formulations and discussing the significant aspects which highlight the role of different geometrical and mechanical parameters to the overall response of RC members in compression. They found that since the reliability of each model depends each time from the specific geometrical and mechanical conditions encountered, the choice of one rather than

another model should pass on an adequate knowledge of the mechanical hypotheses provided by each of them. [Montuori et al., 2012] have analyzed the results of eleven different structural sections dealing with various constitutive laws for reinforced concrete elements confined with FRP. One of the main problems of such constitutive laws is their dependence not only on concrete class, fiber type and wrapping's number of sheets, but on cross-section's size too. They found that, for sections subjected to axial load only, the ultimate strength exhibits the same variability highlighted in this paper for the constitutive laws; conversely in case of members subjected to axial force and bending the part of the concrete section subjected to high compression stresses which, therefore, takes advantage from confinement effects appears quite low so that a significant reduction of the scatter coming from the application of different constitutive models is expected. [Montuori et al., 2013] have investigated the influence of the adopted confined concrete constitutive law, on the flexural strength and curvature ductility of reinforced concrete sections strengthened by FRP (fibre reinforced polymer) wrapping.
The results show that even if the different constitutive laws exhibit large differences in the resulting stress–strain behavior, they lead to negligible differences in terms of flexural resistance, but to very significant differences in terms of curvature ductility. Therefore, the accurate evaluation of the ultimate strain seems of paramount importance compared to the whole stress–strain curve. They have pointed out that to identify the most appropriate stress–strain confinement model, particularly in terms of ultimate strain, it should be adopted to analyse the ultimate response of FRP wrapped reinforced concrete columns subjected to axial force and bending. In addition, the influence of pre-existing loads showing that it affects the knee region of the moment–curvature relationship, while the ultimate flexural resistance remains almost unaffected.

2 Research Significance

It is clear that aspect ratio, slenderness ratio, strength of in-filled concrete, strength of steel, cross-sectional shape and loading cycles are some of the parameters that affect the behavior of CFT columns. Numbers of studies are available for concrete in-filled composite columns with limited work on static lateral or cyclic lateral loading. Still, there is a need for numerical study to check the parameters, which affect the ultimate strength of CFTs. In addition, since the effect of cross section has a significant role in improvement of strength of columns, therefore, some new steel tube sections are proposed in the current study as shown in Figures 1.a, 1.b and 1.c. It is required to understand the behavior of suggested CFT columns under cyclic loading and there is a necessity to enhance the ductility and energy absorption capacity of them. The obtained results of analyses have been compared with the results of previously published numerical studies of CFT columns [Abedi et al., 2008].

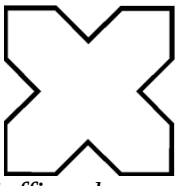

Figure 1.a- *Soffit polygonal section*

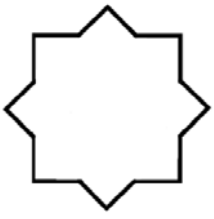

Figure 1.b- *Extrados polygonal section*

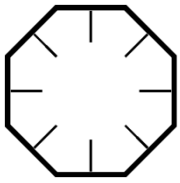

Figure 1.c- *Octagonal section with stiffeners*

3 Finite Element Modelling

[Kwon and Spacone, 2002] mentioned that the finite element method is a powerful tool to effectively simulate the behavior of CFT columns. While simplified analyses that use either beam elements or two-dimensional finite elements are quite useful, only three-dimensional analyses can fully represent all the aspects of the response of CFT structures. In order to understand the structural behavior of CFT columns and carry out comparative investigation under axial and cyclic loadings, geometric and material nonlinear finite element analyses have been undertaken. The models were simulated using ANSYS 10.0 finite element software, which is a general-purpose finite element program designed specially for advanced structural analysis.

3.1 Characteristics of models

[ANSYS R 10.0, 2005] elements and capabilities are as follows.
SOLID65 was used for modelling of concrete which is a 3-D solid element. This element can be used with or without reinforcing bars. This element is capable of cracking in tension and crushing in compression, plastic deformation and creep. A three dimensional solid element (SOLID 45) has been used to model the steel wall, steel tube, and steel stiffeners. The element has plasticity, stress stiffening, large deflection and large strain capabilities. CONTAC52 (for the modelling of gap between steel and concrete) represents two surfaces that might maintain or break physical contact or might slide relative to each other. The element is capable of supporting only compression in the direction normal to the surfaces and shear (Coulomb friction) in the tangential direction. The element might be initially preloaded in the normal direction or be given a gap specification. A specified stiffness acts in the normal and tangential directions when the gap is closed and not sliding. Two-dimensional shell elements (SHELL 43) have been used to model the rigid plate for load applying. This element is well suited to model linear, wrapped, and moderately thick shell structures. A three-dimensional spar element (LINK 8) has been used to model the reinforcement steel of concrete. This element is a uniaxial tension-compression element with three degree of freedom at each node. Plasticity, stress stiffening, and large deflection capabilities are included.

3.2 Material characteristic

The stress-strain behavior of in-filled concrete and the steel wall, used for material and geometric static analyses according to [Schneider, 1998, Mursi and Uy, 2003] is given in Figures 2.a and 2.b, respectively.
For the concrete element, the elastic modules (Ex=26541.38), the Poisson's ratio ($\nu_{xy} = 0.2$), the values for the ultimate tensile strength (f_r=3.72) and ultimate compressive strength

(f_c=35) are the properties of isotropic material as shown in Figure 2.a. Considering Figure 2.b, the behavior of steel is characterized with an initial linear elastic portion of stress-strain relationship with a modulus of elasticity, 209 GPa and up to the yield stress f_y (ST 37 with F_u=370 $^{N}/_{mm^2}$), is equal to 240 MPa, followed by a strain plateau of varying length (strain=0.015) and a following region of strain hardening.

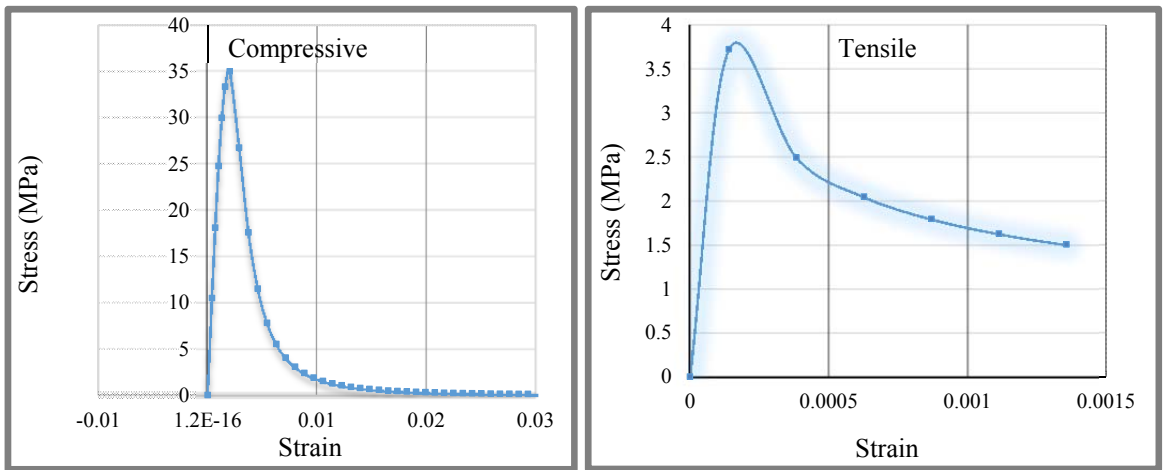

Figure 2.a- *Compressive and tensile stress-strain relationship for un-confined concrete material*

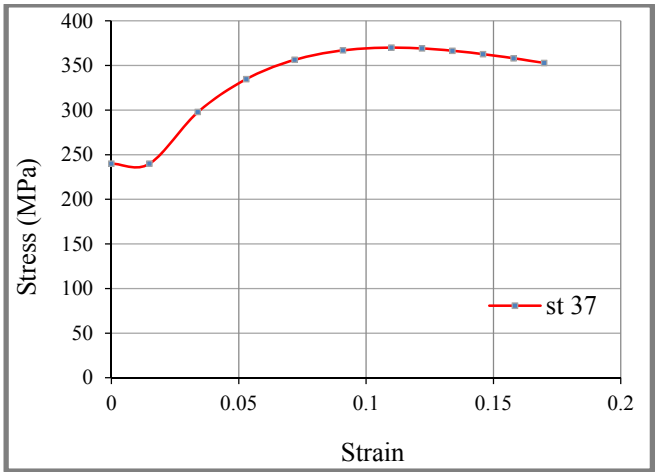

Figure 2.b- *Stress-strain relationship for steel material*

3.3 Verification of the finite element modelling

3.3.1 Verification of the finite element modelling under axial loading

The numerical results attained through material and geometric nonlinear static analyses have been compared with the available experimental results of [Schneider, 1998] to determine the accuracy and validity of the finite element modelling. The summary of experimental specimens' material strength has been presented in Table 1 and it shows material and geometric properties of the specimens where L is the height of column, D is diameter of circular cross section, t is the thickness of steel tube, F_y is the yield stress of steel, E_s is the elastic module of steel, f'_c is the specified stress of concrete, and E_c is the elastic module of

concrete. By carrying out nonlinear structural analysis, numerical result was compared with experimental data. Figure 3 illustrates the experimental and numerical axial load-axial displacement responses under monotonically axial compressive loading. Considering these results, it shows that the theoretical behavior of finite element static analysis, followed closely the actual behavior exhibited by the experimental model and it is concluded that the finite element model is reliable enough to be used in nonlinear analyses for investigating the mechanical behavior and comparing the strength of different types of CFT specimens under axial loading.

Table 1- *Dimensions and material properties of CFT test specimen under axial loading (after Schneider, 1998)*

Sp. NO.	Shape	Length (mm)	Diameter (mm)	Actual Thickness (mm)	Steel properties		Concrete properties	
					f_y (MPa)	E_s (MPa)	f_c' (Kpa)	E_c (MPa)
C1	Cir	605.44	140	3.00	285	189475	28180	25599

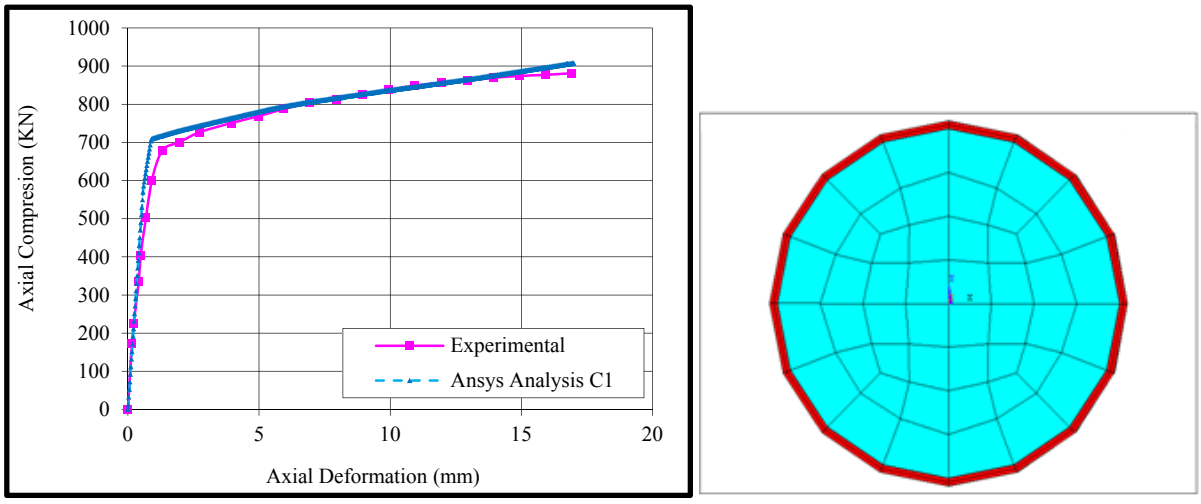

Figure 3- *Axial load- axial deformation curve of C1 specimen under axial loading (Comparison of numerical analysis with the test results of a Schneider, 1998)*

3.3.2 Verification of the finite element modelling under lateral cyclic loading

In order to verify the accuracy and validity of the finite element modelling under lateral cyclic loading, the experimental test results of a previously published test specimen by [Chang et al., 2012] were used and compared with the numerical results obtained from material and geometric nonlinear static analysis for calibration of analyses. The geometrical and material parameters for the test specimen are summarized in Table 2. In this table f_{y1} and f_{y2} are yield strengths for the steel tube and the section steel, respectively. For concrete, f_{cu} is the strength of cube.

Table 2- *Geometrical and material properties of test specimen under lateral cyclic loading (after Chang et al., 2012)*

Specimen ID	Section steel			Steel tube		Concrete properties	
HC12-1	I_{steel}	A_s (mm2)	f_{y1} (MPa)	f_{y2} (MPa)	D×t (mm)	f_{cu} (MPa)	n
	112	3570	314	269	218*4	74.3	0.5

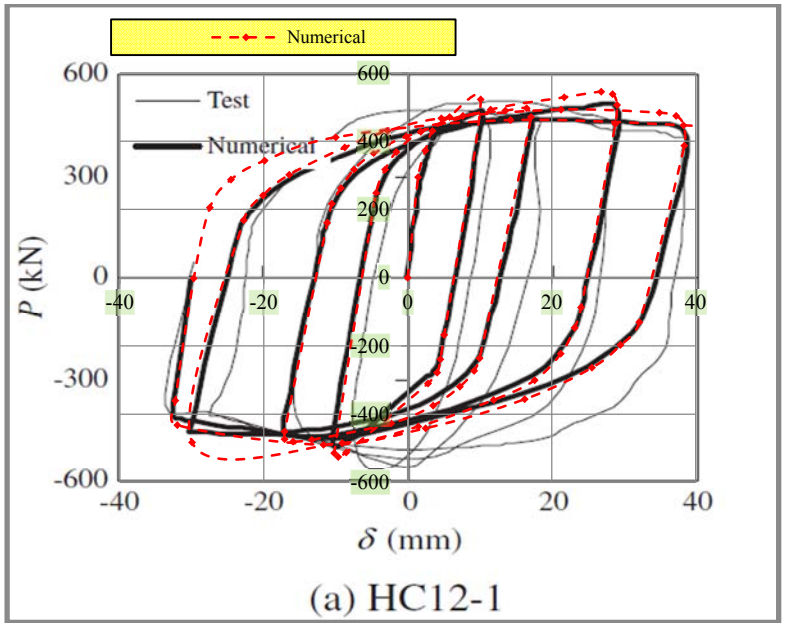

Figure 4- *Comparison of lateral force-displacement curves between numerical and test results of HC12-1 specimen by Chang et al., 2012*

Figure 4 gives the comparison of computed cyclic load (P) versus lateral deflection (δ) curve with the test one. A comparison between hysteresis loops of test result and FE modelling lateral load-displacement curve in this figure, indicates that the maximum lateral load and displacement; degradation of shear strength towards the enclosed area of loops of FEM technique are fairly close to experimental data and they were in reasonable agreement. Contour plots after FEM analysis, including Von-Mises stress contour plot of column model, Von Mises stress in middle part of column, Stress variation of steel elements, Hinge equivalent plastic, were illustrated in Figure 5 (a), (b), (c), and (d), respectively.

The higher stress at the column base caused flexural cracking started at the early stages of loading and the number of flexural cracks increased and propagated with increasing in drift ratios. Therefore, the numerical result of CFT column subjected to lateral cyclic loading was in good agreement with experimental data to estimate the maximum lateral load capacity of columns. This confirms that the present numerical model can be used with confidence to simulate the behavior of CFT columns under lateral cyclic loading.

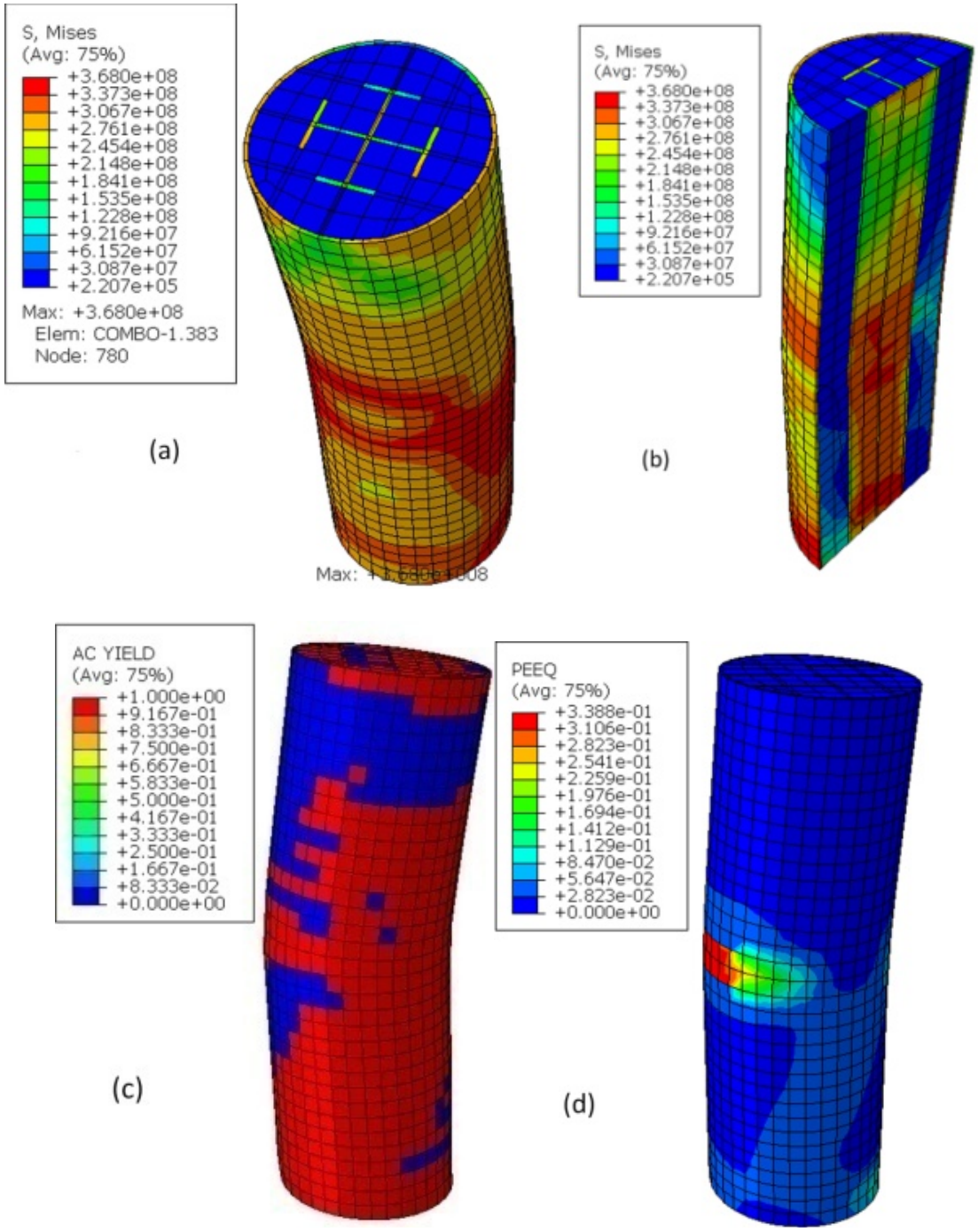

Figure 5- *Contour plots after FEM analysis. (a) Von-Mises stress contour plot of column model; (b) Von Mises stress in middle part of column (c); Stress variation of steel elements; (d) Hinge equivalent plastic*

4 Specifications of Specimens

Nine CFT columns, divided into two groups, have been considered for analyses as shown in Figures 6, and 7. The first group included Po.S20 (twenty-sided polygonal soffit section with filled concrete), Po.E20 (twenty-sided polygonal extrados section with filled concrete),

Po.S12 (twelve-sided polygonal soffit section with filled concrete), Po.E12 (twelve-sided polygonal soffit section with filled concrete), and Sq. (square section with filled concrete).

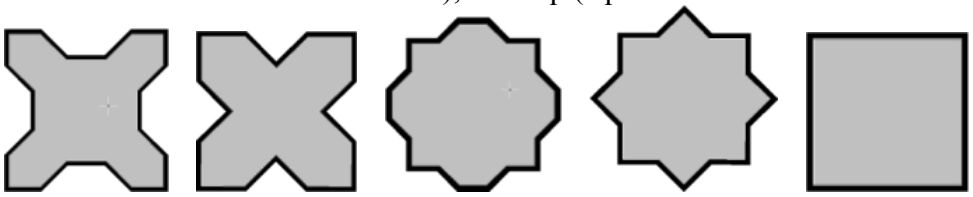

Po.S20 Po.E20 Po.S12 Po.E12 Sq

Figure 6- *Cross section area of first group of CFT columns*

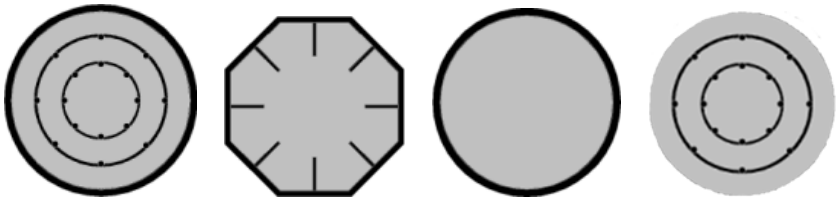

Cir.rc Oct.st Cir rc

Figure 7- *Cross section area of second group of CFT columns*

The second group included Cir.rc (circular section with filled concrete and reinforcement bars), Oct.st (octagonal section with filled concrete and stiffeners), Cir (circular section with filled concrete) and rc (reinforced concrete). For the selection of these sections, some assumptions were applied which are given below.

The assumptions made in the selection of these sections are as follows:

The total cross-section area of the steel (the sum of steel wall, stiffeners and reinforcement bars), concrete core, as well as the material properties in each group are the same and equal.

The selected CFT columns have been considered as columns with common used dimensions and with high load carrying capacity (L=3000 mm).

In each group, the total cross-section area of steel is 23047 mm^2, the cross-section area of concrete is 204282 mm^2.

For steel wall the uniaxial yield stress of steel is 280 MPa (F_y^s), elastic modulus of the steel is equal to 200,000 MPa (E_s).

For concrete compression strength of the unconfined concrete column is 35.0 MPa (f_c'), and elastic modulus of concrete is 31600 MPa (E_c).

In suggested novel sections, area of the stiffeners is 30% of the cross-section area of steel section.

The thickness of steel wall has been selected according to the design provisions, presented by [ACI and AISC], in such a way that the local buckling does not occur in lower loads.

Table 3- *Specifications of first group of CFT columns*

Sample	Po.S20	Po.E20	Po.S12	Po.E12	Sq	Po.S20
Outer Diameter /Width(mm)	551	560	515	624	477.45	551
Thickness of wall(mm)	8.99	11.78	9.42	11.01	12.42	8.99

Table 4- *Specifications of second group of CFT columns*

Sample	Cir.rc	Oct.st	Cir	rc
Outer Diameter /Width(mm)	536.45	534.71	538	524
Thickness of wall(mm)	12.45	9.115	14	-----
Longitudinal reinf.bars	16Ø24	-----	-----	16Ø24
Lateral reinf.bar	Ø10 at 300 mm	-----	-----	Ø10 at 300
Thickness of stiffness(mm)	-----	8.15	-----	-----
Width of stiffness(mm)	-----	110	-----	-----

5 Numerical Results of CFT Columns under Axial Loading

A CFT column can be loaded in the three major ways as shown in Figure 8. Load applying to the steel section only, load applying to the concrete core only, and load applying to the entire section. In both cases, two rigid plates transfer the columns' load, located in the top and bottom of the columns. In the case of load application types of (a) and (b); the axial load was applied to the entire section and concrete core, respectively, and in the case of load application type of (c), the load was applied to the steel section.

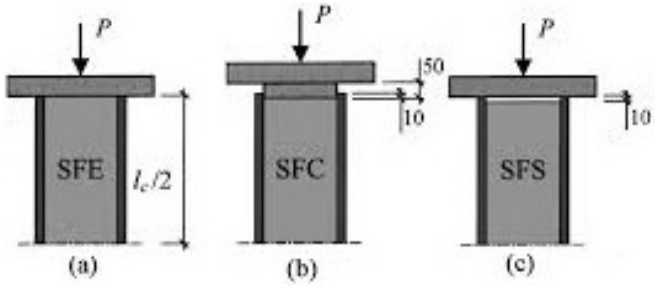

Figure 8- *Load applied to; (a) The entire section, (b) the concrete core, (c) the steel section*

Figures 9.a and 9.b show the axial load–axial displacement responses of first and second groups of CFT columns under axial loading, respectively. The loads have been applied to the entire section (load application type (a)). First group of CFT columns has been selected to investigate the effect of increment of the number of polygonal section sides under axial loading. It was found that with increase in the number of polygonal sections sides, there is no a noticeable difference on the ultimate compressive strength of CFT columns. Therefore, by considering the analyses results, those three specimens (Po.S20, Po.E20) are not economical and applicable and they have been ignored for the next analyses. Considering Figure 9.b, it was found that, under axial loading, polygonal soffit sections show better performance regarding to strength and post buckling behavior in comparison with polygonal extrados and square sections. (Load applied to the entire section). From Figure 9.a, it is observed that the yield load and stiffness of the suggested Polygonal Soffit section (Po.S12) and Octagonal stiffened section (Oct.st) are higher than that of traditional CFT sections. The results clearly show that in polygonal and octagonal sections, the contact stress between steel and concrete causes higher compressive strength, a larger region of permanent axial strength, and a lesser degradation of strength at larger axial displacements. Therefore, the confining effects of new suggested steel sections are higher than traditional ones.

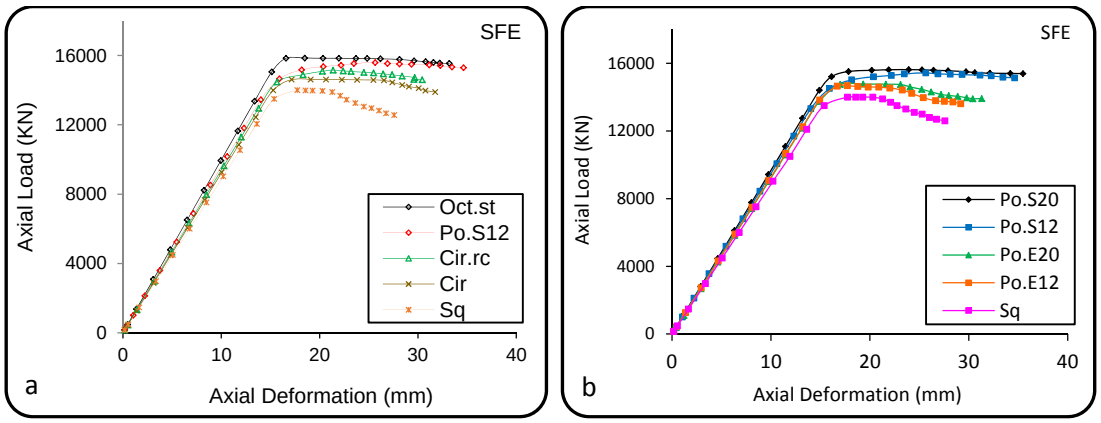

Figures 9- *Axial load–axial displacement responses of CFT columns (load application type of (a), (SFE))*

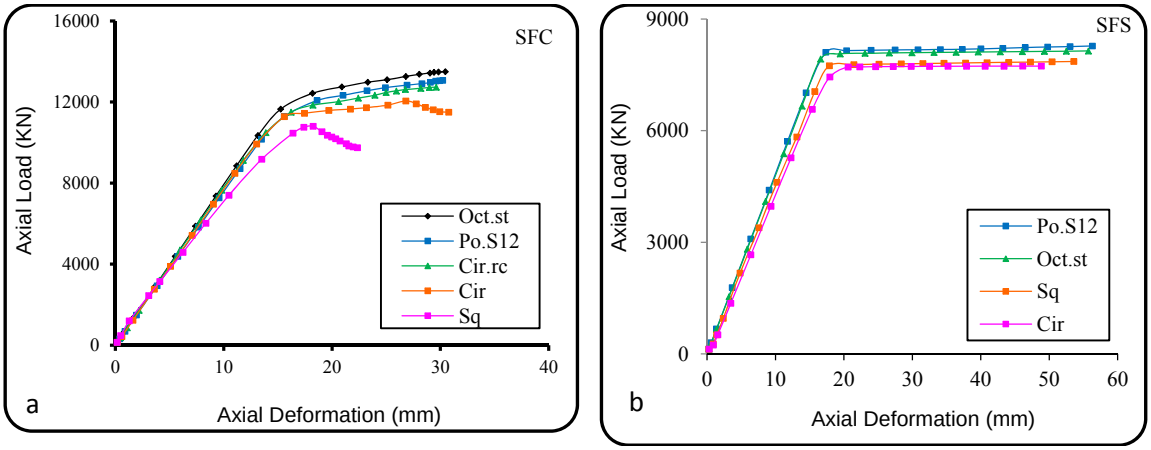

Figure 10- *a) Axial load–axial displacement responses of CFT columns (load application type of (b) (SFC)); b) Axial load–axial displacement responses of CFT columns (load application type of (c) (SFS))*

Figure 10.a shows comparison between CFT samples when load have been applied to the concrete core only (load application type (b)). It shows that the strength and post buckling behavior of suggested sections (Oct.st, Po.S12) is considerably higher than that of traditional CFT columns. Figure 10.b shows axial load–axial deformation responses of CFT columns when load applied to the steel section only (load application type of (c)). It indicates the efficiency of steel wall corners on the critical buckling load of steel sections. Therefore, the Polygonal Soffit section (Po.S12) has higher critical buckling load in comparison with the Octagonal stiffened section (Oct.st) and traditional CFT steel sections.

[Shanmugam and Lakshmi, 2001] mentioned that in the ideal form, in the load application type to the concrete core that would be the appropriate method in the case of lack of bond between steel wall and concrete core. The steel tube only will be applied to confine the concrete core and will not carry any longitudinal stresses. According to the results obtained from Figures 9 and 10, in the case of applying load to the entire section, the results show that the strength of samples in the case of applying load to the entire section is considerably

higher than those samples which load applied to the steel or concrete section only. But, in the case of applying load to the concrete core only, the samples exhibit appropriate strain-hardening characteristics on their post-yield behavior.

6 Numerical Results of CFT Columns under Eccentric Loading

In order to investigate the behavior of CFT column under eccentric loading, a circular column type with the characteristics and eccentricity of the load provided in Table 5 was investigated and the load-deflection curves and moment- rotation curves of end of each column were compared in Figures 11.a and 11.b, respectively. In Figures 11.a and 11.b, it can be seen that in loads with eccentricity of more than 2, due to the minor axial force versus moment, there is no loss of load bearing capacity in the column, and only the column is bent under the load of moment.

Table 5- *The characteristics and load eccentricities of CFT specimen under eccentric loading*

Specimen	Shape of section		Diameter (mm)		Tube thickness (mm)		f_y (MPa)		E_s (MPa)		$f_c^{'}$ (MPa)		E_C (MPa)		L (mm)
C-CFT	Circle		300		6		240		2E5		40		3E4		4000
e/D	0.0	0.1	0.2	0.3	0.4	0.5	0.6	0.7	0.8	1	2	3	4	5	10

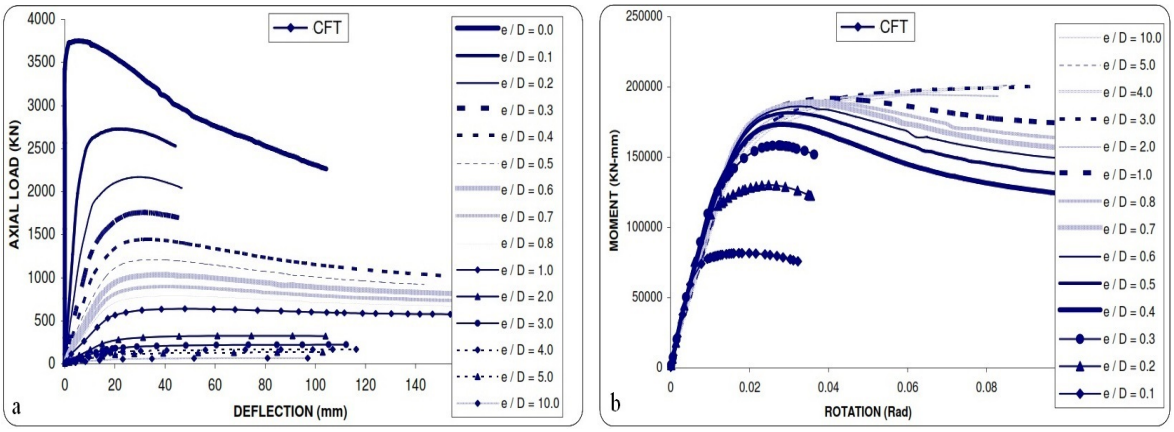

Figure 11- *a) Load-deflection comparison curves of CFT columns; b) Moment- rotation comparison curves of CFT columns*

In Figure 12.a, the moment of each column is obtained from the multiplication of the axial load at the eccentricity of load. As expected, with the increase in eccentricity of load, the load bearing capacity of the column decreases. In order to indicate the moment-axial force interaction curve, in Figure 12.a, the axial force and the maximum moment capacity of each column are represented by a point, and by connecting them to each other, the failure push curve of the column is obtained under axial load and moment. Also, in order to better understand the drop in load bearing capacity of column with the increase of the load eccentricity, a non-dimensional curve is drawn. It is obtained by dividing the values of the horizontal axis of the curve of Figure 12.a into the maximum moment (in the case of a pure moment loading, when the eccentricity of load (e / D = 10) and dividing the values of its

vertical axis into the maximum axial load (in the state without eccentricity e / D = 0) as shown in Figure 12.b.

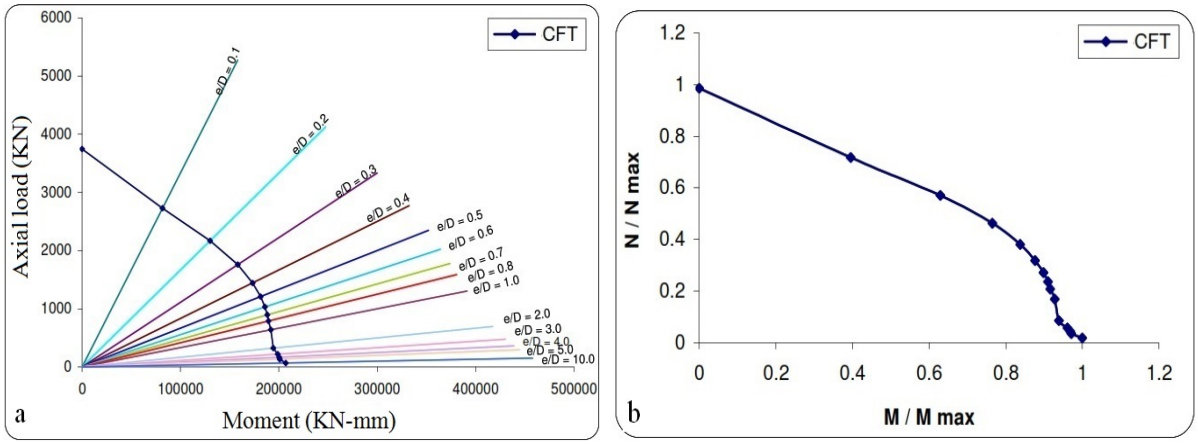

Figure 12- *a) Moment- axial load interaction curve of CFT columns; b) Normalized moment-axial load interaction curve of CFT columns*

With reference to Figure 13.a, in order to obtain a relationship for calculating the maximum moment capacity of a column under the specified axial load, the formula No.1 is suggested for the calculating of the normalized moment- axial load interaction curve of CFT column.

$$m = \frac{(1-2n+n^2)}{(1-n-0.79n^2+0.795\,n^3)} \qquad (1)$$

$$m = \frac{M}{M_{max}} \quad , \quad n = \frac{N}{N_{max}}$$

Which in that M_{max} is Maximum moment in pure moment loading state, and N_{max} is Maximum axial load in state of axial loading without eccentricity of load.

In order to ensure the accuracy of the relationship, a comparison between the numerical interaction curve and the curve obtained from the above equation is shown in Figure 13.a. As can be seen, the obtained relation has an acceptable accuracy, and the relation until the eccentricity amount of 0.9 (e/D = 0.9) is slightly conservative and then slightly unstable.

In order to indicate the effect of load eccentricity on the load bearing capacity of CFT columns, the amounts of axial load to the maximum axial load bearing capacity of columns, for the different load eccentricities are shown in Figure 13.b. As can be seen, up to the eccentricity amount of 1 (e/D=1), the amount of load loss (about 80 %) is strongly affected by the load eccentricities, while for the load eccentricities more than 1, the sensitivity of the column to load eccentricity has decreased and the load loss is not tangible. By using this graph, the column load drop under the axial load, could be achieved with any amount of eccentricity. For example, for the eccentricity amount of 1(e / D = 1), the load drop is about 80%. Considering Figure 13.b, in order to calculate the load drop in CFT columns under eccentric loading, the formula No.2 is proposed for the investigation of effect of load eccentricity on the load reduction percentage of CFT columns.

$$n = \frac{1}{(1+5(^{e}/_{D}))} \qquad (2)$$

$$n = \frac{N}{N_{max}}$$

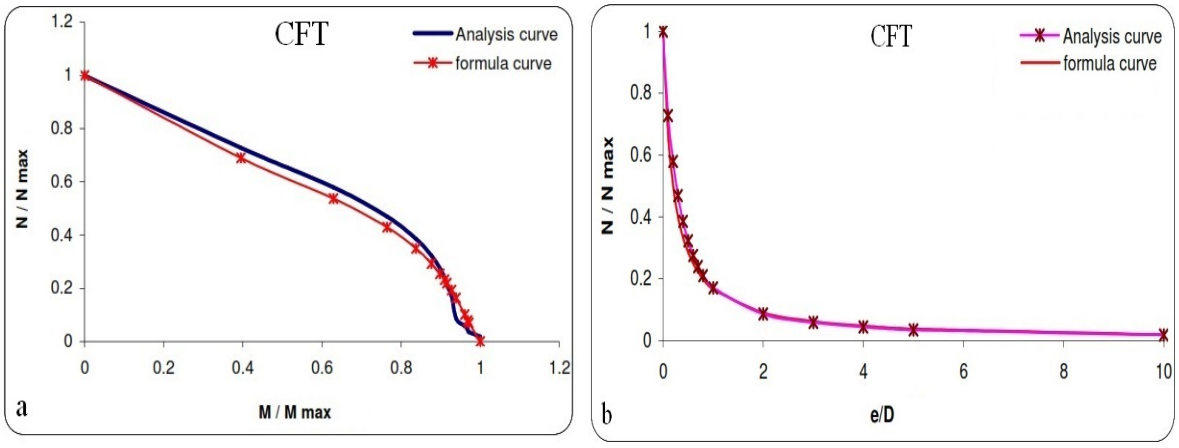

Figure 13- *a) The comparison between the analysis interaction curve and the curve obtained from the formula No. 1 in the CFT columns; b) The comparison of the effect of load eccentricity on the load reduction percentage of CFT columns by the analysis curve and the curve obtained from the formula No. 2.*

7 Numerical Results of CFT Columns under Lateral Cyclic Loading

In concrete-filled steel tubular beam-columns under lateral cyclic loadings, local buckling of the steel tube, crushing and slipping of the confined concrete according to [Bai et al., 2016] could have important role on the degradation of strength and stiffness of CFT columns. In order to investigate the effects of steel tubes on the hysteretic behavior of reinforced concrete (rc) columns, according to Table 4, two specimens (rc and Cir.rc) were selected. First, a monotonic axial load equal to $0.3.f'_c.A_g$ was applied on the top nodes of the column. Then, displacement history according to [Hajjar and Goerley, 1997] was applied to model the condition of lateral cyclic loading as shown in Figure 14.a. Figure 14.b is schematically showing boundary condition of specimens and the manner of applying the lateral cyclic loading.

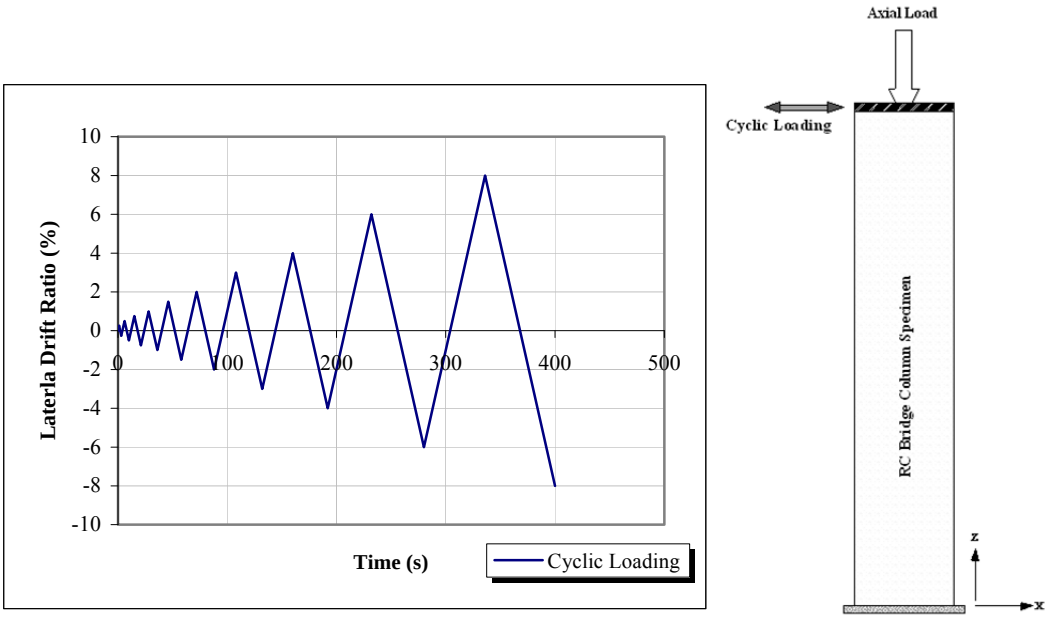

Figure 14- *a) History of hysteretic loading; b) Boundary condition*

7.1 Hysteretic behavior of Cir.rc and rc specimens

The behavior of the specimens has been shown in the form of a lateral force-displacement hysteretic relationship. The hysteretic curves for Cir.rc and rc specimens are demonstrated in Figure 15. Considering Figure 15, the maximum shear strength of the rc specimen was about 859 kN, which was considerably less than the shear strength of its corresponding nominal flexural capacity. Damages in the base of the columns' concrete element in "pull" direction causes a loss of load bearing capacity of the specimen.

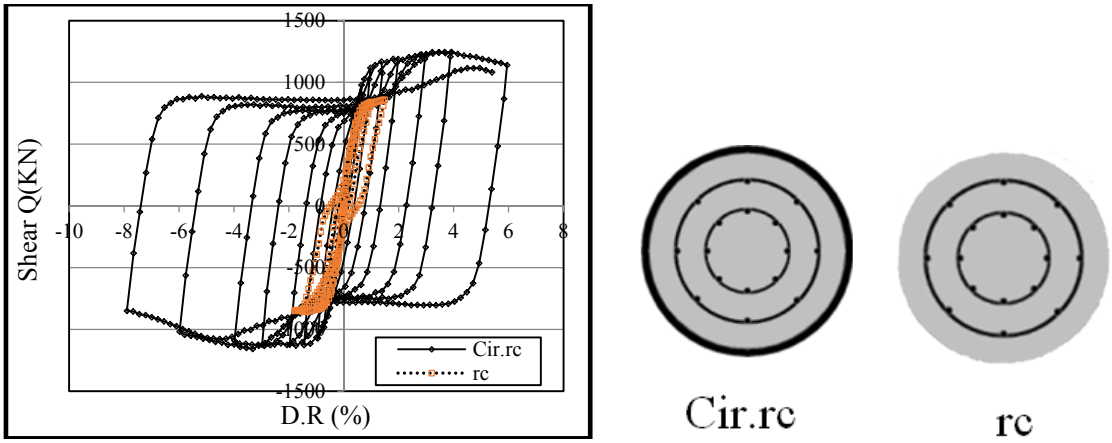

Figure 15- *The hysteretic loops for Cir.rc and rc specimens under lateral cyclic loading*

In the Cir.rc specimen, the maximum shear strength equal to 1247 KN was achieved in drift ratio of 2%, which is more than its nominal flexural resistance. The considerable load loss in the "pull" direction between drift ratio of 2% and 4% obtained because of the failure of longitudinal bars at the base of the column. The shear strength of relative displacement is linear up to the second cycle of loading and in the fourth to sixth cycles of loading, inelastic deformation happened without significant loss of load. Consequently, using circular steel tube for reinforced concrete column (Cir.rc) caused columns to absorb higher rates of energy under cyclic displacement history. Shear strength of CFT column was increased and the degradation of shear strength of specimen occurred at larger lateral drift ratio in comparison with rc specimen. This suitable performance is relevant to an increment in the total area of steel part; increment of concrete confinement covered by steel reinforcement, and obtained abeyance at cracking of concrete.

7.2 Hysteretic behavior of CFT columns

To indicate the effect of steel section shapes on the hysteretic behavior of CFT column according to Tables 3 and 4, four samples have been selected. The hysteretic curves of CFT columns have been illustrated in Figures 16.a and 16.b.

Considering Figure 16.a, it is indicated that the maximum shear strength in Polygonal Extrados specimen (Po.E12) is 1376 kN where as this quantity for Octagonal stiffened specimen (Oct.st) is equal to 1270 kN. Figure 16.b indicate that the degradation of strength in circular section filled with reinforced concrete (Cir.rc) began suddenly at 4% of lateral displacement, while considering Figure 16.a, the shear strength of polygon section (Po.E12) inclined toward an increasing slope.

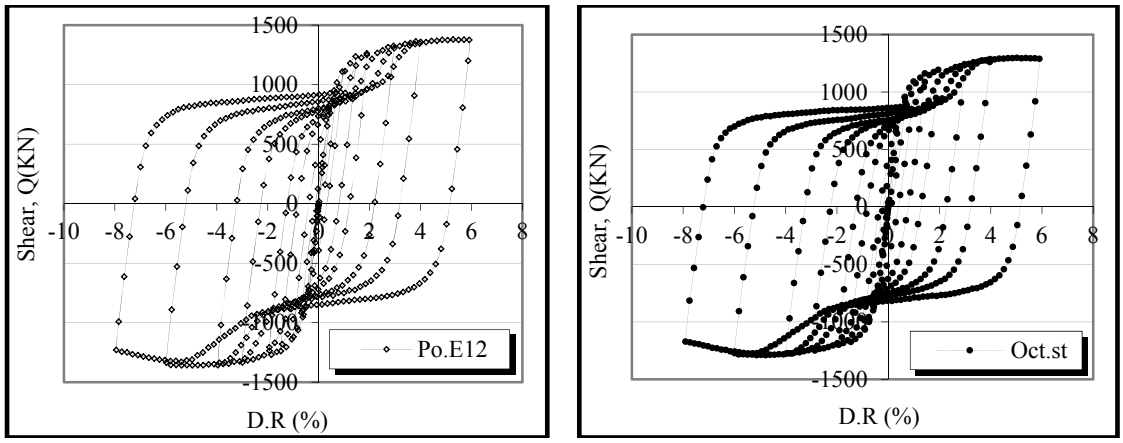

Figure 16- *a) The hysteretic loops for Po.E12-Oct.st specimens under lateral cyclic loading*

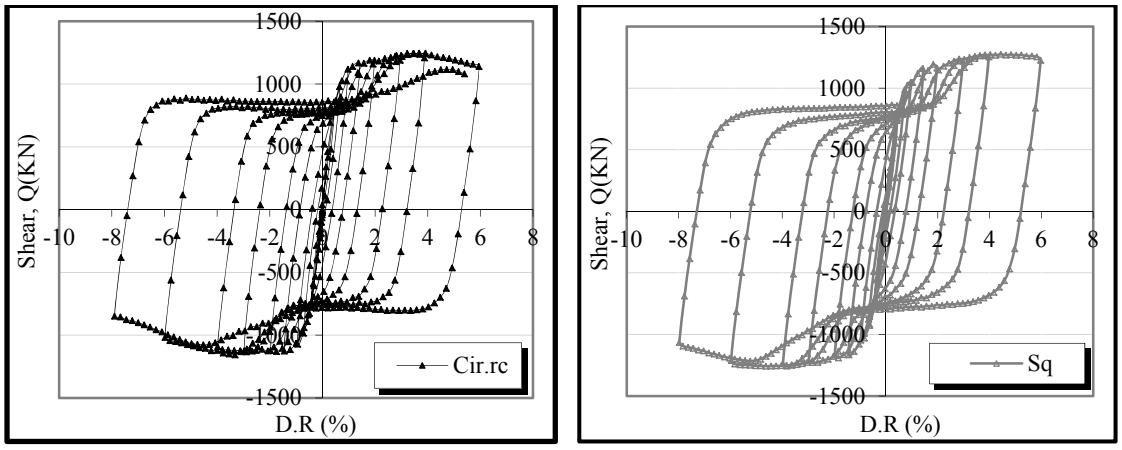

Figure 16- *b) The hysteretic loops for Cir.rc-Sq specimens under lateral cyclic loading*

7.3 Comparison of hysteresis loops of CFT columns

Figure 17 illustrates the lateral load-displacement envelopes for the comparison between CFT samples. Each point of the envelope is the maximum shear force carried by the column in each corresponding cycle of loading. Considering Figure 17, it was found that the proposed polygonal extrados section leads to more significant results, the lesser degradation of load and higher shear strength compare to the previous configurations of CFT columns under lateral cyclic loading. In addition, the polygonal soffit section (Po.S12) has the minimum shear strength among CFT specimens.

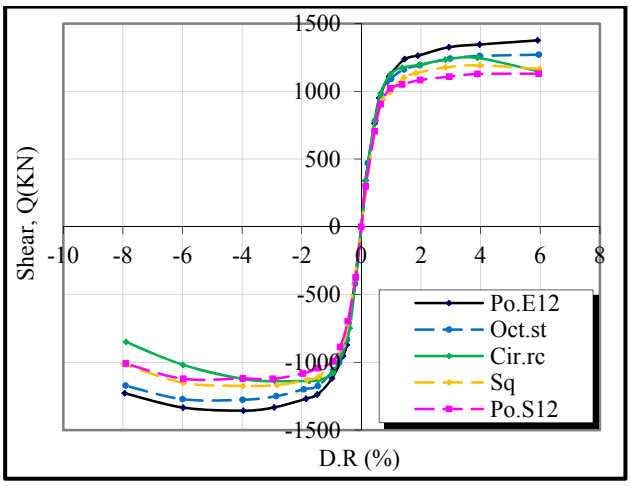

Figure 17- *The envelope curves of hysteretic loops for CFT specimens*

7.4 Energy dissipation

The elastic plastic deformation is generally quantified by ductility parameters and by energy dissipation capacity. The ability of a structure to survive earthquake conditions depends mostly on its ability to dissipate the input energy. Various energy forms in structures include kinetic energy, damping energy, elastic energy, hysteretic energy and input energy. [Gobarah et al., 1997] mentioned that an effective way for evaluation and comparison of CFTs behaviors is studying the effects of different parameters onto the hysteretic energy dissipation curves. The area enclosed by the corresponding load-displacement hysteretic curve is a criterion for dissipated energy in any particular cycle of loading.. Despite energy dissipation calculated as described did not represent the total energy dissipated by the specimens; it can be used for comparison purposes. Figure 18 illustrates the comparison of energy dissipation diagram of CFT columns in each loading cycle. The diagram clearly shows that the amount of energy absorbed in suggested sections are considerably higher than that of traditional CFT sections.

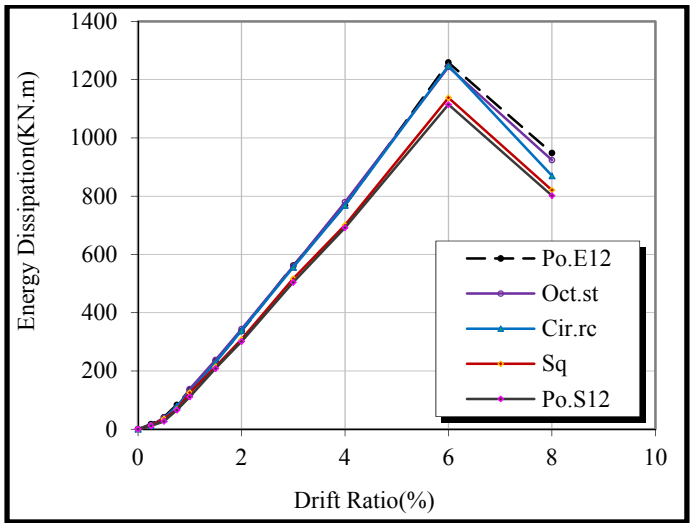

Figure 18- *Energy dissipated- lateral drift ratio of CFT specimens*

Considering the values of energy dissipation parameter, Polygonal Extrados section (Po.E12) showed almost a 10 % improvement in comparison with square CFT section. For plastic stiffness in cycle No. 9 of loading, a minimum of 5% increase was exhibited against the square specimen. It is evident from the results given in Table 6 that the suggested shapes have higher shear strength, absorbing energy capacity, and appropriate ductility characteristics than that of common CFT columns. It is indicated that under lateral cyclic loading, the Polygonal Extrados specimen (Po.E12) has the best performance regarding stiffness, ductility, and energy absorption capacity among the samples. From the other hand, the Polygonal Soffit section (Po.S12) has the worst performance regarding stiffness, ductility, and energy absorption capacity, whilst under axial loading it has almost the appropriate performance regarding the ultimate compressive strength of CFT columns.

Table 6- *Comparison of effective parameters of CFT columns*

Specimen	Maximum Shear Strength (kN)	Ratio	Energy dissipated (kN.m)	Ratio	Stiffness plastic (N/mm)	Ratio
Sq	1191	1.00	1138	1.00	409	1.00
Po.S12	1127	0.94	1114.5	0.98	404	0.99
Cir.rc	1246	1.04	1243.5	1.09	413	1.01
Oct.st	1270	1.06	1248	1.09	419	1.02
Po.E12	1376	1.15	1259	1.10	430	1.05

Considering the values of energy dissipation parameter, Polygonal Extrados section (Po.E12) showed almost a 10 % improvement in comparison with square CFT section. For plastic stiffness in cycle No. 9 of loading, a minimum of 5% increase was exhibited against the square specimen. It is evident from the results given in Table 6 that the suggested shapes have higher shear strength, absorbing energy capacity, and appropriate ductility characteristics than that of common CFT columns. It is indicated that under lateral cyclic loading, the Polygonal Extrados specimen (Po.E12) has the best performance regarding stiffness, ductility, and energy absorption capacity among the samples. From the other hand, the Polygonal Soffit section (Po.S12) has the worst performance regarding stiffness, ductility, and energy absorption capacity, whilst under axial loading it has almost the appropriate performance regarding the ultimate compressive strength of CFT columns.

8 Summary and Conclusions

In this paper a new kind of CFT columns with octagonal and polygonal section shapes has been proposed. To make a comparative investigation into the effects of various steel section (polygonal and octagonal) shapes on the mechanical and hysteretic behavior of CFT columns, the numerical results of nonlinear static analyses have been verified with the experimental result of CFT columns under axial and lateral cyclic loading. It was found that the finite element model is reliable enough to be applied in nonlinear analyses. Strength and hysteresis behavior of the suggested new steel sections have been investigated and the quantitative comparison between some parameters such as the maximum shear strength, energy dissipated, and the plastic stiffness of CFT samples have been investigated. This study evidenced that

new proposed CFT columns can be used in seismic region and it can provide a proper background for the practical engineering applications.
Followings are the conclusions:
1. Under axial loading in the CFT columns, the efficacy of shape of steel section on the increment of concrete strength due to the confinement phenomenon is considerable for octagonal stiffened and polygonal soffit sections.
2. Under axial loading in the CFT columns, the compressive strength and post buckling behavior of octagonal stiffened and polygonal soffit sections are higher than those of the common sections are.
3. Under eccentric loading in the CFT columns, up to the eccentricity amount of 1 (e/D=1), the amount of load loss is strongly affected by the load eccentricities, while for the load eccentricities more than 1, the sensitivity of the column to load eccentricity has decreased and the load loss is not tangible.
4. Under lateral cyclic loading in the CFT columns, the suggested polygonal extrados section has the best performance regarding stiffness, ductility, and energy dissipation capacity rather than the common CFT samples. In addition, the obtained results indicate lesser degradation of load at the subsequent cycles for the suggested CFT section, whilst, the Polygonal Soffit section (Po.S12) showed the worst performance in comparison with all CFT samples.
5. Using circular steel tube for reinforced concrete column (Cir.rc) caused that circular CFT specimen absorbs more energy in comparison with reinforced concrete (rc). The shear strength of circular CFT specimen was increased and the degradation of shear strength of the specimen occurred at larger lateral drift ratio in comparison with the specimen without steel tube (reinforced concrete, (rc)).

References

Abedi, K., Ferdousi, A., Afshin, H. (2008). A novel steel section for concrete-filled tubular columns. Thin-Walled Structures, 46: 310–319.

ACI. (1995). American Concrete Institute (ACI), ACI Building code requirements for reinforced concrete, ACI standard 318.

AISC/LRFD. (2001). American Institute of Steel Construction/ Load and Resistance Factor Design, Manual of steel construction," (AISC/LRFD) standard 2001-11-01. 3rd.

ANSYS R 10.0. (2005). Academic, Structural analysis Guide.

Bai, Y., Lin, X., Mou, B. (2016). Numerical modelling on post-local buckling behavior of circular and square concrete-filled steel tubular beam columns. International Journal of Steel Structures, 16(2): 531–546.

Cavaleri, L., Trapani, F.D., Ferrotto, M.F., Davì, L. (2017). Stress-strain models for normal and high strength confined concrete: Test and comparison of literature models reliability in reproducing experimental results. Ingegneria Sismica, 34(3-4): 114-137.

Chang, X., Wei, Y.Y., Yun, Y.C. (2012). Analysis of steel-reinforced concrete-filled steel tubular (SRCFST) columns under cyclic loading. Construction and Building Materials, 28: 88–95.

Chitawadagi, M.V., Narasimhan, M.C., Kulkarni, S.M. (2010). Axial strength of circular concrete-filled steel tube columns – DOE approach. Journal of Constructional Steel Research, 66(10): 1248–1260.

Chithira, K., and Baskar, K. (2012). Experimental and numerical investigation on circular CFT columns under eccentric load condition with and without shear connectors. International Journal of Earth Sciences and Engineering, 05(01): 169-179.

Clotilda, P., Hanizah, A.H., Azmi, I., Gerard, P. (2010). Experimental behavior of concrete filled thin walled steel tubes with tab stiffeners. Journal of Constructional Steel Research, 66(7): 915-922.

Clotilda, P., Hanizah, A.H., Azmi, I., Joe, D.N. (2011). Bond strength in concrete filled built-up steel tubes columns with tab stiffeners, Canadian Journal of Civil Engineering, 38(6): 627-637.

Clotilda, P., Hanizah, A.H., Azmi, I., Joe, D.N. (2016). Behavior of eccentrically loaded slender concrete filled steel tubes columns. Jurnal Teknologi, 78(5–4): 13–17.

Dario, L. M., Giordano, L., Castaldo, P., Gino, D. (2017). Assessment of the efficiency of seismic design for structural robustness of RC structures. Ingegneria Sismica, 34(3-4): 63-77.

Endo, T., Shioi, Y., Hasegawa, A., Wang, H. (2014). Experimental study on reinforced concrete filled steel tubular structure. Steel and Composite Structures, 17(4): 517-533.

Galano, L., and Vignoli, A. (2008). Strength and ductility of HSC and SCC slender columns subjected to short-term eccentric load. ACI Structural Journal, 105(3): 259-270.

Gardner, N.J., Godse, R.G., Wong, T.F. (1992). Laterally prestressed eccentrically loaded slender columns. ACI Structural Journal, 89(S51): 547-555.

Gobarah, A., Biddah, A., Mahgoub, M. (1997). Rehabilitation of reinforced concrete columns using corrugated steel jacketing. Journal of Earthquake Engineering, 4(1): 651-673.

Gopal, S.R., and Manoharan, P.D. (2006). Experimental behavior of eccentrically loaded slender circular hollow steel columns in-filled with fibre reinforced concrete. Journal of Constructional Steel Research, 62(5): 513-520.

Hajjar, J.F., and Goerley, B.C. (1997). A cyclic nonlinear model for concrete filled tubes- formulation. Journal of structural Engineering, 123(6): 736-744.

Hamidian, M.R., Jumaat, M.Z., Alengaram, U.J. RamliSulong, N.H., Shafigh, P. (2016). Pitch spacing effect on the axial compressive behavior of spirally reinforced concrete-filled steel tube (SRCFT). Thin-Walled Structures, 100: 213–223.

Hua, W., Wang, H.J., Hasegawa, A., Shioi, Y., Iwasaki, S., Miyamoto, Y. (2005). Study on strength of reinforced concrete filled circular steel tubular columns. Structural Engineering, 19: 653–677.

Kwon, M., and Spacone E. (2002). Three-dimensional finite element analyses of reinforced concrete columns. Computers & Structures, 80: 199-212.

Mete, E., Ayşegül, G., Mermerdaş, K. (2016). Ultimate capacity prediction of axially loaded CFST short columns. International Journal of Steel Structures, 16(1): 99–114.

Montuori, R., Piluso, V., Tisi, A. (2012). Comparative analysis and critical issues of the main constitutive laws for concrete elements confined with FRP, Composites Part B: Engineering, 43 (8): 3219-3230.

Montuori, R., Piluso, V., Tisi, A. (2013). Ultimate behavior of FRP wrapped sections under axial force and bending: Influence of stress-strain confinement model. Composites Part B: Engineering, 54 (1): 85-96.

Montuori, R., and Piluso, V. (2015). Analysis and modelling of CFT members: Moment curvature analysis. Thin-Walled Structures, 86: 157-166.

Morino, S., Uchikoshi, M., Yamaguchi, I. (2001). Concrete filled steel tube column system its advantages. Steel Structures, 1: 33-44.

Mursi, M., and Uy, B. (2003). Strength of Concrete Filled Steel Box Columns Incorporating Interaction Buckling. Journal of Structural Engineering, 129(5): 626-639.

Qin, P., and Xiao, Y. (2013). Research on concrete-filled steel tube columns subjected to cyclic lateral force. The world congress on Advances in Structural Engineering and Mechanics (ASEM13), Jeju, Korea.

Rangan, B.V., and Joyce, M. (1992). Strength of eccentrically loaded slender steel tubular columns filled with high strength concrete. ACI Structural Journal, 89(6): 676-681.

Rides, J.M., Lu, L.W., Sooi, T.K., Vermaas, G. (1996). Seismic performance of CFT column-to-WF beam moment connections. Connections in steel structures III: Behavior, Strength and Design, 99-114.

Shanmugam, N.E., and Lakshmi B., (2001). State of the art report on steel–concrete composite columns. Journal of Constructional Steel Research, 57: 1041–1080.

Schnabl, S., Jelenić, G., Planin, I. (2015). Analytical buckling of slender circular concrete-filled steel tubular columns with compliant interfaces. Journal of Constructional Steel Research, 115: 252–262.

Schneider, S.P. (1998). Axially loaded concrete-filled steel tubes. ASCE Journal of Structural Engineering, 124(10): 1125-1138.

Uenaka, K. (2014). Experimental study on concrete filled elliptical/oval steel tubular stub columns under compression. Thin Wall Structures, 78: 131–7.

Xiamuxi, A., and Hasegawa, A. (2011). Compression test of RCFT columns with thin-walled steel tube and high strength concrete. Steel Composite Structures, 11: 391–402.

Xiamuxi, A., and Hasegawa, A. (2012). A study on axial compressive behaviors of reinforced concrete filled tubular steel columns. Journal of Constructional Steel Research, 76: 144–154.

ingegneria sismica
International Journal of Earthquake Engineering
Anno XXXV – Num. 3

STUDI NUMERICI RELATIVI A COLONNE CON SCATOLARI IN ACCIAIO RIEMPITI DI CALCESTRUZZO SOGGETTE A CICLI DI CARICO ASSIALE, ECCENTRICO E LATERALE

Ebrahim Farajpourbonab[1]

[1]Department of Civil Engineering, University of Pune, Pune, (M.S.), India

SUMMARY: Il lavoro presenta uno studio numerico, realizzato mediante il programma di calcolo ANsys, relativo a colonne scatolari in acciaio riempite di calcestruzzo soggette a carichi ciclici assiali, eccentrici e laterali. I risultati teorici sono stati confronti con osservazioni sperimentali. Al fine di migliorare il comportamento di questi elementi strutturali, in questo lavoro viene proposta un particolare tipo di rinforzo per la sezione in acciaio. Sono stati realizzati 8 prove sperimentali con diverse sezioni. I risultati mostrano che la proposta formulata nel lavoro consente di ottenere un significativo incremento sia di resistenza che di duttilità.

KEYWORDS: *CFT column, compressive strength, Octagon and Polygons steel sections, FE analysis, hysteretic behavior*

Corresponding author: Ebrahim Farajpourbonab, Department of Civil Engineering, University of Pune, India.
Email:farajpourbonab@gmail.com